Aeolian transport of sand

M.P. Almeida[1], J.S. Andrade Jr[1], and H.J. Herrmann[1,2,a]

[1] Departamento de Física, Universidade Federal do Ceará, 60455-900 Fortaleza, Ceará, Brazil
[2] Institute for Building Materials, ETH Zurich, Switzerland

Abstract. The airborne transport of particles on a granular surface by the saltation mechanism is studied through numerical simulation of particles dragged by turbulent air flow. We calculate the saturated flux q_s and show that its dependence on the wind strength u_* is consistent with several empirical relations obtained from experimental measurements. We propose and explain a new relation for fluxes close to the threshold velocity u_t, namely, $q_s = a(u_* - u_t)^\alpha$ with $\alpha \approx 2$. We also obtain the distortion of the velocity profile of the wind due to the drag of the particles and find a novel dynamical scaling relation. We also obtain a new expression for the dependence of the height of the saltation layer as function of the strength of the wind.

PACS. 45.70.Mg Granular flow: mixing, segregation and stratification – 47.55.Kf Particle-laden flows – 47.27.-i Turbulent flows – 83.80.Hj Suspensions, dispersions, pastes, slurries, colloids

1 Introduction

Aeolian transport of sand is the key factor in sand encroachment, dune motion and determines coastal and desert landscapes. Saltation is the dominating transport mechanism as first described by Ralph Bagnold [1]. It consists of grains being lifted upwards, accelerated by the wind and finally impacting onto the ground producing a splash of new ejected particles. Reviews can be found in references [2,3]. The quantitative understanding of this process is however still incomplete.

The wind looses more momentum the more particles it carries until a saturation is reached. The maximum number of grains a wind of given strength can carry through a unit area per unit time defines the saturated flux of sand q_s. This flux has been measured many times in wind tunnel experiments and in the field, and various empirical expressions describing its dependence on the wind strength have been proposed in the past [4–9]. Also theoretical expressions have been derived using approximations for the drag in turbulent flow [10,11]. Most relations are given by polynomials in the friction speed u_* which are of third order using the assumption that the grain hopping length scales with u_* [4,5,10–12]. Some expressions are also more complex [6]. The velocity profile modified by a layer of particles has also been measured [13,14] and modelled [15]. Interestingly however only few measurements of the height of the saltation layers as function of u_* have been reported [16,17] and no systematic data are available close to the threshold. A comprehensive analytical treatment of

this problem remains out of reach on one hand because of the turbulent character of the wind and on the other hand due to the moving boundary conditions required to solve the equations of motion. Recently, a deterministic model for aeolian sand transport without considering height dependence in the feedback has been proposed [18] in which two types of moving grains (saltons and reptons) coexist. In this language we will here only consider saltons. Despite the efforts made in the past [19] there remain many uncertainties about the trajectories of the particles and their feedback with the velocity field of the wind. It is this challenge which motivated the present work and led us to discover a scaling relation for the distorted velocity profile and a new dependency of the flux close to the threshold.

We present in this paper a numerical study of saltation which solves the turbulent wind velocity field and its feedback with the dragged particles [20–22]. We will neither consider temporal fluctuations in the velocity field nor different particle sizes. The advantage is that as a consequence, we will be able to determine all quantities with higher precision than ever before, and therefore achieve a better resolution close to the critical velocity at which the saltation process begins.

2 Model

It is our aim to reproduce as realistic as possible the conditions encountered in wind channel experiments. For that purpose we simulate the layer of airborne particle transport above a granular surface inside a two-dimensional
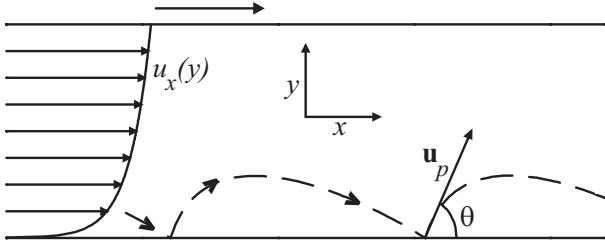
Fig. 1. Schematic illustration of the set-up showing the mobile wall at the top, the velocity field at different positions in the y-direction and the trajectory of a particle stream (dashed line). At the collision between this stream and the static wall at the bottom, we consider that the particles rebound to the air flow at an ejection angle θ, with only a fraction r of their original kinetic impact energy.

channel with a mobile top wall as we can see schematically in Figure 1 to avoid distortion of the wind profile at the top.

Between the left and the right side we impose a pressure gradient. Gravity points down, i.e., in negative y-direction. The y-dependence of the pressure drop is adjusted in such a way that a logarithmic velocity profile is insured along the entire channel in the case without particles, as is expected in fully developed turbulence [23]. More precisely, we ensure that the profile follows the form

$$u_x(y) = (u_*/\kappa)\ln(y/y_0), \qquad (1)$$

u_x being the component of the wind velocity in the x-direction, u_* the shear velocity or wind strength, $\kappa = 0.4$ the von Kármán constant and y_0 the roughness length which is typically between 10^{-4} and 10^{-2} m. We used in our simulation $y_0 = 1.5 \times 10^{-4}$ m. We move the upper wall of the channel with a velocity equal to the velocity of the wind profile of equation (1) at that height imposing in this way a non-slip boundary condition.

Inside the channel we assume that we have an incompressible Newtonian fluid flowing under steady-state and homogeneous turbulent conditions. The fluid we chose is air having a viscosity $\mu = 1.7894 \times 10^{-5}$ kg m^{-1} s^{-1} and a density $\rho = 1.225$ kg m^{-3}. The Reynolds-averaged Navier-Stokes equations in the version of the standard $k - \epsilon$ model are used to describe turbulence. The numerical solution for the velocity and pressure fields is obtained using the commercial software FLUENT which operates through discretization by means of the control volume finite-difference technique [24,25]. The integral version of the governing equations is considered at each cell of the numerical grid to generate a set of non-linear algebraic equations which are pseudo-linearized and solved. The convergence criteria used in the simulations are defined through the residuals, i.e., a measure of the degree up to which the conservation equations are satisfied throughout the entire flow field. In our simulations we consider that convergence is achieved only when each of the normalized residuals is smaller than 10^{-6}.

Once a steady-state turbulent flow is produced, we proceed with the simulation of the particle transport along the channel. We assume that drag and gravity are the only relevant forces acting on the particles and do not consider eventual collisions of particles. Then their trajectories can be obtained by integrating the following equation of motion:

$$\frac{d\mathbf{u}_p}{dt} = F_D(\mathbf{u} - \mathbf{u}_p) + \mathbf{g}(\rho_p - \rho)/\rho_p, \qquad (2)$$

u_p being the particle velocity, $\mathbf{g}$ gravity and $\rho_p = 2650$ kg m^{-3} a typical value for the density of sand particles. The term $F_D(\mathbf{u} - \mathbf{u}_p)$ describes the drag force per unit particle mass where

$$F_D = \frac{18\mu}{\rho_p d_p^2} \; \frac{C_D \mathrm{Re}}{24}, \qquad (3)$$

$d_p = 2.5 \times 10^{-4}$ m being a typical particle diameter, $\mathrm{Re} \equiv \rho d_p |\mathbf{u}_p - \mathbf{u}|/\mu$ the particle Reynolds number, and C_D the drag coefficient taken from an empirical relation [26]. In our simulation each particle represents in fact a stream of many real grains. It is necessary to take into account the feedback on the local fluid velocity due to the momentum transfer to and from the particles. This coupling effect is considered here by alternately solving the particle equations and the fluid equations until the solutions agree in the sense that the local amount of momentum gain of all the particles is equal to the momentum subtracted from the fluid. This momentum transfer is computed by adding the momentum change of every particle as it passes through a control volume [25],

$$\mathbf{F} = \sum_{\text{particles}} F_D(\mathbf{u} - \mathbf{u}_p)\dot{m}_p \Delta t, \qquad (4)$$

$\dot{m}_p$ being the mass flow rate of the particles and Δt the time step. The exchange term equation (4) appears as a sink in the Navier-Stokes equation, i.e. the momentum balance of the fluid.

3 Results

The trajectory of one particle stream and the velocity vectors along the y-direction can be seen in Figure 1. Each time a particle hits the ground it keeps a fraction r of its energy and a new stream of particles is ejected at that position forming an angle θ with the horizontal. The parameters $r = 0.84$ and $\theta = 36°$ are chosen from experimental measurements [27,28]. We also studied other values for r and θ and even considered a continuous distribution of ejection angles. As expected, the choice of unphysical values produces unrealistic results.

If u_* is below a threshold value u_t the energy loss at each impact prevails over the energy gained during the acceleration through drag and particle transport comes to a halt. If the particle has an initial energy this one decreases at each impact so that the jumps become lower each time until the trajectory ends on the ground as illustrated in Figure 2. Only for $u_* > u_t$ steady sand motion can be achieved. The resulting flux is given by

$$q = \dot{m}_p n_p, \qquad (5)$$
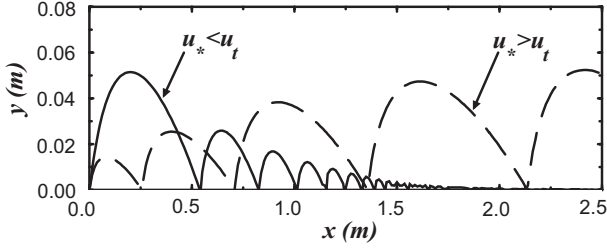
Fig. 2. Typical trajectories of fixed number of particles computed for $u_* < u_t$ (full line) and $u_* > u_t$ (dashed line).

n_p being the number of particle streams released. In fact, if the initial energy is below the one of steady state the first added particle streams are strongly accelerated in the channel and their jumping amplitude increases after each ejection until a maximum is reached as seen in Figure 2. This is a transitional phenomenon.

One can also at fixed wind strength u_* vary the sand flux by changing the amount of mass — or equivalently the number of particles — in a trajectory. The more particles are injected the smaller is the final height of the trajectories. Beyond a certain number n_p of particle streams, the trajectories however start to loose energy and the overall flux is reduced. This critical value n_p characterizes the saturated flux q_s through equation (5). We see this situation in Figure 3. When the flux is saturated the trajectory attains a perfectly periodic motion after a short transient of several jumps. If less mass is transported the trajectory keeps slowly increasing in height. In a wind tunnel new grain trajectories would be created for an unsaturated flux, but in our model the number of trajectories n_p is fixed and since also for a given simulation the mass per simulation does not change in time the trajectories keep increasing. Let us note that the fact that in Figure 3 some trajectories don't seem to touch the ground is only a graphic artifact due to the discretization.

In Figure 4 we see the plot of q_s as function of the wind velocity u_*. Clearly, there exists a critical wind velocity threshold u_t below which no sand transport occurs at all. This agrees well with experimental observations [1,5,29]. Also shown in Figure 4 is the best fit to the numerical data using the classical expression proposed by Lettau and Lettau [5],

$$q_s = C_L \frac{\rho}{g} u_*^2 (u_* - u_t), \qquad (6)$$

C_L being an adjustable parameter. We find rather good agreement using fit parameters of the same order as those of the original work [5] and a threshold value of $u_t = 0.35 \pm 0.02\,\mathrm{m/s}$. This is in fact, to our knowledge, the first time a numerical calculation is able to quantitatively reproduce this empirical expression supporting in this way the validity of our simulation method. Other empirical relations from the literature [10–12] have also successfully been used to fit these results. In Figure 4 we also show that for large values of u_* asymptotically one recovers cubic dependence on u_* that was already proposed by Bagnold [4].
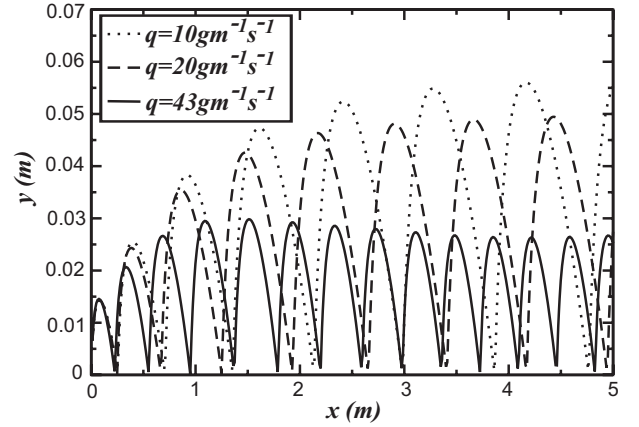
Fig. 3. Particle trajectories for three different values of mass flow rate $q = 10\,\mathrm{g\,m^{-1}\,s^{-1}}$ (dotted line), $q = 20\,\mathrm{g\,m^{-1}\,s^{-1}}$ (dashed line), and $q = q_s = 43\,\mathrm{g\,m^{-1}\,s^{-1}}$ (full line), in a saturated flow which has $u_* = 0.5064$ in the absence of particles. The slight decrease of the height at q_s is just a transient behaviour.
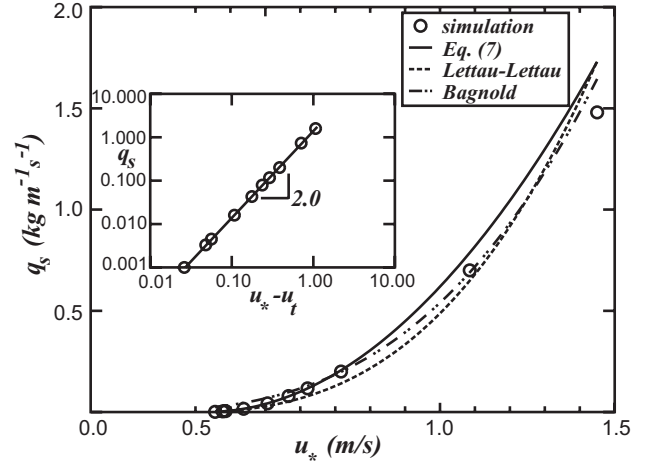

Fig. 4. Plot of the saturated flux q_s as function of u_*. The dashed line is the fit using the expression proposed by Lettau and Lettau [5], $q_s \propto u_*^2 (u_* - u_t)$, with $u_t = 0.35 \pm 0.02\,\mathrm{m/s}$. The full line corresponds to equation (7) and the dashed-dotted line to Bagnold's relation, $q_s \propto u_*^3$ [4]. The results shown in the inset (log-log plot) confirm the validity of the the power-law relation equation (7), $q_s \propto (u_* - u_t)^2$, with the critical point given by $u_t = 0.33 \pm 0.01\,\mathrm{m/s}$.

What is, however, unexpected and striking is that close to the critical velocity u_t we find that a parabolic expression of the form

$$q_s = a(u_* - u_t)^2 \qquad (7)$$

fits the data better than equation (6), as can be seen in Figure 4 and in particular in the inset. This quadratic law of equation (7) might be due to the fact that the shear stress at the ground can be decomposed into a dynamical and a turbulent part, $\tau = \tau_d + \tau_T$, the first being proportional to ηu_* and the second proportional to $\mu(u_* - u_t)$, where η and μ are the dynamical and the turbulent viscosities. In the limit $u_* \gg u_t$ one obtains the classical
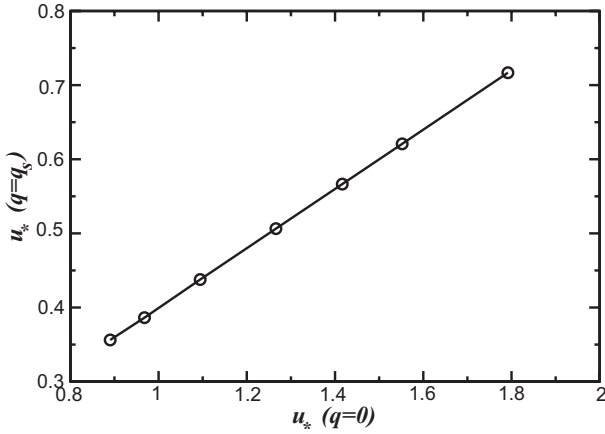
Fig. 5. Plot of u_* at the saturated mass flow condition ($q = q_s$) against its value in a pure flow without particle $q = 0$.

asymptotic behavior of Bagnold [4], as verified by the dash-dotted line in Figure 4 and which is consistent with references [5,10–12]. The limit $u_* \approx u_t$, however, yields the quadratic relation for the flux given in equation (7). The physical reason for this seems to be that close to u_t the laminar component of the boundary layer cannot be neglected. We conclude that in fact the full dependence of q_s on u_* is essentially an extrapolation between the quadratic law close to u_t given by equation (7) and Bagnold's asymptotic cubic behaviour for large u_*. All proposed empirical laws in some way fulfill this purpose.

Because of the feedback of particle motion on the wind velocity field, i.e. the momentum loss of the fluid due to Newton's second law, the wind strength is substantially weakened when carrying a saturated flux. One can actually define the wind strength $u_*(q = q_s)$ at the saturated mass flow condition by fitting its profile $u_x(y)$ for large heights y to a logarithm as given by equation (1). Interestingly this new weakened wind strength $u_*(q = q_s)$ depends linearly on the undisturbed wind strength $u_*(q = 0)$ as seen in Figure 5 but is less than have as strong. It would be very interesting to check this prediction experimentally in a wind tunnel.

The velocity profile of the wind within the layer of grain transport is experimentally much more difficult to access than the sand flux. Close to the ground this profile clearly deviates very much from the undisturbed logarithmic form of equation (1) because of the momentum that the fluid must locally yield to the particles. In Figure 6 we show the height (y) dependent loss of velocity with respect to the logarithmic profile without particles of equation (1) for different values of q. As seen clearly in Figure 6, for a given wind strength u_* the loss of velocity is maximal at the same height y_{max}, regardless of the value of the flux q. Except for large values of the flux, dividing the velocity axis by q one can collapse all the profiles quite well on top of each other as can be verified in the inset of Figure 6. This shows that the loss of momentum of the wind is as expected proportional to the amount of grains it carries.

The difference between the disturbed and the disturbed profile at the saturated flux $q_s(u_*)$ is shown in
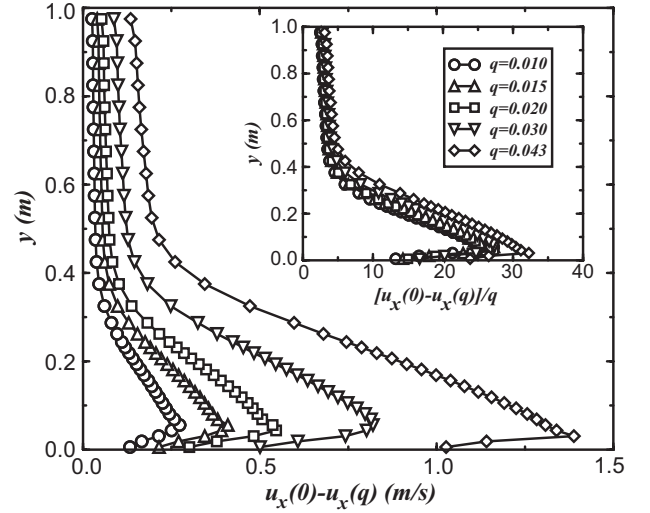
Fig. 6. Profile of the velocity difference $u_x(0) - u_x(q)$ for different values of the flux q at fixed $u_* = 0.51$ m/s. The flux is changed by changing the mass per trajectory. Only the leftmost curve corresponds to the saturated flux q_s. The inset shows the data collapse of these data obtained by rescaling the velocity difference with the corresponding q.
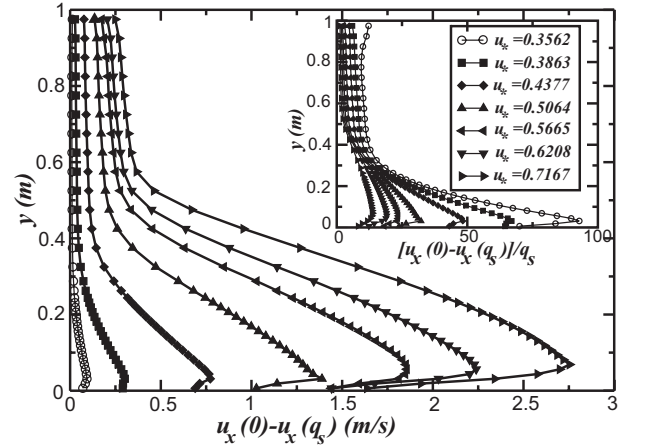
Fig. 7. Difference between the velocity profiles of a flow without particle ($q = 0$) and with maximum particle flow mass ($q = q_s$), for different flow conditions expressed by the value of u_* in the flow with $q = q_s$. In the inset we have these differences divided by their respective saturated mass flow rate q_s.

Figure 7 for different wind strengths u_*. The shapes of the profiles are similar to each but a good collapse cannot be achieved by rescaling of the horizontal axis dividing by the value of $q_s(u_*)$ as seen in the inset of Figure 7. This is due the non-linearity of the function $q_s(u_*)$ (see Fig. 4). The deviation of a collapse gets stronger close to the threshold u_t. The height y_{max} at which the loss of momentum is largest does clearly increase with u_*.

The height y_{max} at which the momentum loss is maximized depends essentially linearly on u_* as shown in Figure 8. This is consistent with the observation that the saltation jump length is proportional to u_* [11] because the height of a saltation trajectories is proportional to its
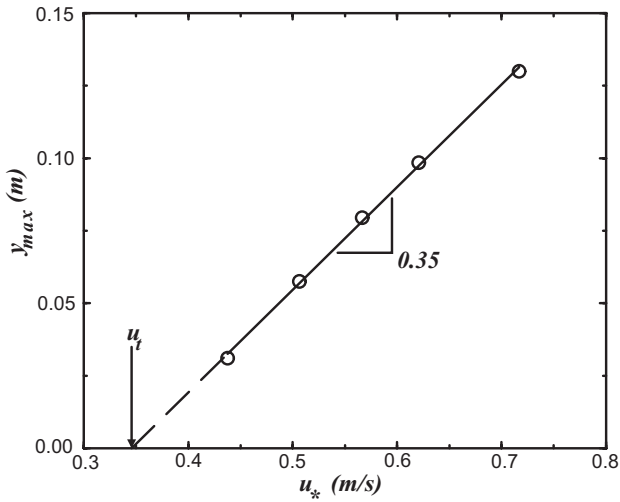
Fig. 8. Height y_{max} of the maximum loss of velocity as function of u_*. The height y_s of the largest probability to find a particle coincides with y_{max}. The solid line corresponds to the best linear fit to the data with a slope equal to 0.35. By extrapolation, the intercept with the x-axis provides an alternative estimate for the critical point, $u_t = 0.35\,\mathrm{m/s}$, that is consistent with the other calculations.

length. We get from Figure 8:

$$y_{max} = 0.35[s]\ \ (u_* - u_t).\qquad(8)$$

Quantitatively the results in Figure 8 also agree very well with the experimental data of reference [16] and are consistent with analytical arguments of given by Sørensen [11]. Extrapolating to $y_{max} = 0$, we obtain an alternative estimate for the threshold velocity, $u_t = 0.35\,\mathrm{m/s}$, that is consistent with the values calculated before by fitting our data to equations (6) and (7) in Figure 4.

If one goes to the desert or to a beach during a very windy day one realizes that the saltation process in nature looks like a sheet of particles floating above the ground at a certain height y_s which strongly depends on the wind velocity. This height seems to correspond to the position of the largest likelihood to find a particle as obtained from the maximum of the density profile of particles as function of height y. Figure 8 implies that the profile of velocity difference of the wind has a minimum at a similar height, which is consistent with the maximal loss of momentum. Within the error bars our results in fact yield that y_s coincides with the values of y_{max} in Figure 8. It is important to note that both heights, y_{max} and y_s, also have the same linear dependence on u_*.

4 Conclusion

In this paper we have shown results of simulations of the layer of granular transport in a turbulent air flow. The lack of temporal fluctuations allows for a precise study close to the critical threshold velocity u_t that leads us to discover a parabolic dependence of the saturated flux on the wind strength. Compared to wind tunnel measurements our numerical value for u_t is rather high which is probably due to the fact that we do neglect time dependent fluctuations in the velocity due to turbulence. We also show that the velocity profile disturbed by the presence of grains scales linearly with the flux of grains but not with the wind strength. Notably a characteristic height appears at which the momentum loss in the fluid and therefore the grain density are maximal. This height increases linearly with the wind velocity u_*. The present model can be extended in many ways including the study of the dependence of the aeolian transport layer on the grain diameter, the gas viscosity, and the solid or fluid densities. This does allow to calculate, for instance, the granular transport on Mars and compare with the expression presented in reference [12]. Work in this direction has been done and will be published soon [30].

Several of our findings could also be tested experimentally in wind tunnel experiments. On one hand the linear dependence between the wind strength at saturation on the undisturbed wind strength as shown in Figure 5 should be easily verifiable. Careful measurements close to the threshold u_t might also be able to check the quadratic dependence of the saturated flux on u_* given in equation (7).

References

1. R.A. Bagnold, *The Physics of Blown Sand and Desert Dunes* (Methuen, London, 1941)
2. R.S. Anderson, M. Sørensen, B.B. Willetts, Acta Mech. (Suppl.) **1**, 1 (1991)
3. H.J. Herrmann, in *The Physics of Granular Media*, edited by H. Hinrichsen, D. Wolf (Wiley VCH, Weinheim, 2004), pp. 233–252
4. R.A. Bagnold, Proc. R. Soc. Lond A **167**, 282 (1938)
5. K. Lettau, H. Lettau, in *Exploring the World's Driest Climate*, edited by H. Lettau, K. Lettau (Center for Climatic Research, Univ. of Wisconsin, Madison, 1978)
6. B.T. Werner, J. Geol. **98**, 1 (1990)
7. K.R. Rasmussen, H.E. Mikkelsen, Acta Mechanica Suppl. 1, **135** (1991)
8. Y.-H. Zhou, X. Guo, X.J. Zheng, Phys. Rev. E **66**, 021305 (2002)
9. J.D. Iversen, K.R. Rasmussen, Sedimentology **46**, 723 (1999)
10. P.R. Owen, J. Fluid Mech. **20**, 225 (1964)
11. M. Sørensen, in *Proc. Int. Wkshp. Physics of Blown Sand* (Univ. of Aarhus, Denmark, 1985), p. 141, Vol. 1; M. Sørensen, Acta Mech. (Suppl.) **1**, 67 (1991)
12. B.R. White, Geophys. Res. **84**, 4643 (1979)
13. G.R. Butterfield, in *Turbulence: Perspectives on Flow and Sediment Transport*, edited by N.J. Cliffod, J.R. French, J. Hardisty (John Wiley, 1993), Chap. 13, p. 305

14. K. Nishimura, J.C.R. Hunt, J. Fluid. Mech. **417**, 77 (2000)
15. J.E. Ungar, P.K. Haff, Sedimentology **34**, 289 (1987)
16. Z. Dong, X. Liu, H. Wang, A. Zhao, X. Wang, Geomorphology **49**, 219 (2002)
17. K.R. Rasmussen, H.E. Mikkelsen, Sedimentology **45**, 789 (1998)
18. B. Andreotti, J. Fluid Mech. **510**, 47 (2004)
19. P. Nalpanis, J.C.R. Hunt, C.F. Barrett, J. Fluid Mech. **251**, 661 (1993)
20. M.P. Almeida, J.S. Andrade Jr, H.J. Herrmann, Phys. Rev. Lett. **96**, 018001 (2006)
21. I.K. McEwan, B.B. Willetts, J. Fluid Mech. **252**, 99 (1993)
22. P.J. Spies, I.K. Mc Ewan, Earth Surf. Proc. and Landforms **25**, 437 (2000)
23. L. Prandtl, in *Aerodynamic Theory*, edited by W.F. Durand (Springer, Berlin, 1935), Vol. III, p. 34
24. S.V. Patankar, *Numerical Heat Transfer and Fluid Flow* (Hemisphere, Washington DC, 1980)
25. The FLUENT (trademark of FLUENT Inc.) commercial package for fluid dynamics analysis is used in this study
26. S.A. Morsi, A.J. Alexander, J. Fluid Mech. **55**, 193 (1972)
27. R.S. Anderson, P.K. Haff, Science **241**, 820 (1988)
28. F. Rioual, A. Valance, D. Bideau, Phys. Rev. E **62**, 2450 (2000)
29. R. Greeley, J.D. Iversen, *Wind as a Geological Process* (Cambridge Univ. Press, 1983)
30. M.P. Almeida, J.S. Andrade Jr, H.J. Herrmann, in preparation